Ultrasonics Sonochemistry 89 (2022) 106122

Contents lists available at ScienceDirect

Ultrasonics Sonochemistry

journal homepage: www.elsevier.com/locate/ultson

The effect of ultrasound on synthesis and energy storage mechanism of Ti_3C_2Tx MXene

Wu Zhang *, Xinyue Zhang

School of Materials Science and Engineering, Shenyang Ligong University, Shenyang, Liaoning 110159, PR China

ARTICLE INFO

Keywords:
Ti_3AlC_2
Removal of Al
Sonochemical synthesis
Ti_3C_2Tx MXene

ABSTRACT

Removal of aluminum (abbreviated to Al) accounts for the main step for synthesizing Ti_3C_2Tx MXene. To date, the synthesis of Ti_3C_2Tx MXene is hampered by the low removal efficiency of Al from Ti_3AlC_2. Ultrasound was therefore introduced to achieve efficient synthesis of Ti_3C_2Tx MXene by promoting the removal rate of Al from Ti_3AlC_2. It was found that ultrasonic aid can significantly boost the removal efficiency of Al. Additionally, distinct kinetics for the removal of Al was recognized as the advent of ultrasonic intervention: (i) the shrinking core model was used to describe the removal kinetics of Al in the case without ultrasound, whilst the shrinking particle model was capable for the case in presence of ultrasound; (ii) the activation energy for removal of Al with ultrasonic aid was 70.2 kJ/mol, indicating a chemical reaction-controlled process, whereas the corresponding value for the case without sonication was 28.1 kJ/mol, demonstrating a mixed kinetic feature of the removal process of Al. Morphological study showed that ultrasound can remove the surface-adhering reaction products and favors the formation of structures with flower-like morphology. The sample without sonication treatment exhibited typical capacitive behavior, whilst the contribution of diffusion-limited capacitance in addition to the capacitive behavior was readily observed for the sonication-treated sample. Surface chemistry study indicated the more prevalent oxidation of the sonication treated sample, which gave rise to a higher specific capacitance than those without sonication treatment.

1. Introduction

MXenes have been identified as promising materials in various fields such as energy storage [1], wave shielding [2], and sensors. Recently, MXenes have been frequently used as electrocatalysts [2,3], and high active electrocatalytic performance has been achieved, which is comparable to metal-based materials [4–7]. MXenes can be prepared from their precursor, named as MAX phase, which has the general chemical formula of $M_{n+1}AX_n$ [8]. In a typical MAX phase, M stands for early transition metals, A denotes an A-group element and X represents C or N, or a combination of them. To date, more than 100 discrete stoichiometric forms of MXenes have been theoretically predicted, and over 30 chemical formulations of MXene have been successfully synthesized [8]. Among the abundant MXenes, Ti_3C_2Tx is the most actively studied one, in which the Tx stands for the surface terminations, such as –OH, -F, and -Cl, etc. Ti_3C_2Tx is normally prepared by selective removal of Al from Ti_3AlC_2 structure, which is named as the etching of Al [8]. In the Ti_3AlC_2 structure, the aluminum (abbreviated to Al) atoms are weakly bonded to the two adjacent layers of Ti_3C_2, this renders the Al atoms chemically active, and therefore the removal of Al can be achieved via chemical reactions. A range of chemical configurations has been demonstrated for synthesizing Ti_3C_2Tx MXene, such as HF, NH_4HF_2, NaOH, LiF in HCl solution, etc [8]. Among these chemical reagents, hydrofluoric acid solution has been proved to be a good candidate for removal of Al from the Ti_3AlC_2 structures.

Synthesis of Ti_3C_2Tx MXene consists of two consecutive steps: (i) removal of Al from the Ti_3AlC_2 precursor; (ii) exfoliation of the multiple-layered Ti_3C_2Tx MXene into single or few-layered structures [9]. The preparation efficiency is kinetically limited by the former process, i.e., removal of Al from Ti_3AlC_2 structures. Although the hydrofluoric acid solution has been proved to be a suitable etchant for synthesizing Ti_3C_2Tx MXene, the scalable production of high-quality Ti_3C_2Tx MXene is still challenging which is primarily due to the low efficiency of the removal of Al from Ti_3AlC_2, typically more than 24 h of removal of Al is needed for complete removal of Al [10]. A variety of strategies have been introduced to improve the removal efficiency of Al, two prime examples are electrochemical and sonication-aided techniques [11,12]. Electrochemically aided removal of Al has been experimentally proved

* Corresponding author.
E-mail address: neusmmzhangwu@163.com (W. Zhang).

https://doi.org/10.1016/j.ultsonch.2022.106122
Received 12 June 2022; Received in revised form 8 August 2022; Accepted 10 August 2022
Available online 13 August 2022

as a viable approach to promote the removal efficiency of Al. However, due to the narrow electrochemical window of the aqueous solution, electrochemically aided removal of Al from Ti_3AlC_2 has to be performed in non-aqueous electrolytes, e.g., molten salt, in which high-temperature and prevention of exposure of the electrolytes from the atmosphere are needed, and this makes the removal process of Al experimentally elusive [13]. In contrast to the electrochemical-aid approach, ultrasound-assisted synthesis of MXenes does not need to be performed at high temperatures and inert atmosphere, which shows minimal requirements for the operating experimental conditions/environments.

Although sonochemical synthesis of Ti_3C_2Tx MXene has been preliminarily proved to be a good alternative to the conventional approaches for the removal of Al from Ti_3AlC_2. Insightful study on the effect of ultrasound on the removal of aluminum from Ti_3AlC_2 and electrochemical performance of the resulting Ti_3C_2Tx MXene is scarce, and the intricacies of the underlying physics and mechanisms are still not clear. Herein, we present a detailed investigation on ultrasound-assisted removal of Al from Ti_3AlC_2, including the variation of morphology, phase composition, surface chemistry of the sample, and the reaction kinetics caused by the introduction of ultrasound. In particular, the alteration of the energy storage mechanism of Ti_3C_2Tx MXene due to the introduction of ultrasound was firstly studied, which benefits the scientific community for the fabrication of MXenes materials.

2. Experimental section

2.1. Materials and instruments

In this work, the Ti_3AlC_2 with a purity of greater than 98 % was purchased from Beijing Forsman Co., ltd., China. The average particle size was determined to be 21.3 μm. Concentrated hydrofluoric acid (49 %), acetylene black, polyvinylidene fluoride, *N*-methylpyrrolidone (NMP), and deionized water were purchased from Sinopharm Chemical Reagent Co., ltd. Sonicators (240 W8151, GTSONIC Co., ltd., China and BILON-650Y, Sonics & Materials, Inc, USA) were used to perform the sonication-based removal experiments and to prepare the solutions with desired concentrations, the diameter of the probe is 2 mm and the depth is 5 cm. Specifically, the experiments with different frequencies were performed using 240 W8151 sonicator, other experiments were performed using the BILON-650Y sonicator. The electrochemical performance of the samples was tested on a CHI 760E (Shanghai CH Instrument, Co., ltd., China) electrochemical workstation. Non-sonicated removal experiments of Al were conducted by using A Heidolph magnetic stirrer (Hei-Tec, Heidolph Instruments, Germany). An X-ray diffractometer with Cu-Kα radiation was used to study the phase composition of the samples. Morphological studies of the samples were performed on a Field Emission Scanning Electronic Microscope. X-ray photoelectron spectra (XPS) of the samples were measured on an ESCALAB 250Xi spectrometer (Thermo Fischer, USA) at a basic chamber pressure of $4 \times l0^{-9}$ mbar. The specific area of the samples is measured by using a nitrogen gas adsorption analyzer (Autosorb-iQ-MP, Quantachrome Instruments, USA. The particle size distribution of the sample was measured on a BT-2000 particle size analyzer (Bettersize, Co., ltd., China). Analysis of Al content in the samples was performed by using an ICP-OES instrument (icap pro, Thermo Scientific, USA).

2.2. Experimental procedure

The Al removal experiments are represented by the following reactions: [14].

$$Ti_3AlC_2 + 3HF = Ti_3C_2 + AlF_3 + 3/2H_2 \quad (1)$$

$$Ti_3C_2 + 2H_2O = Ti_3C_2(OH)_2 + H_2 \quad (2)$$

$$Ti_3C_2 + 2HF = Ti_3C_2F_2 + H_2 \quad (3)$$

Unlike the general removal experiments of Al, removal of Al from Ti_3AlC_2 precursor is usually conducted at slightly elevated temperatures, e.g., 30 ℃, 40 ℃, and 50 ℃, to avoid unwanted reactions. For comparison, the removal experiments of Al are divided into two groups: the experiments with and without sonication. In the case of removal experiments of Al in absence of ultrasound, 2 g Ti_3AlC_2 was added into 50 ml the ice-bathed hydrofluoric acid solution at a rate of ca. 0.2 g/min to prevent extremely rigorous reaction in the mixture. Upon the completion of Ti_3AlC_2 addition, the acquired slurry was heated to the characteristic experimental temperatures. Magnetic stirring at 200 rpm, 400 rpm, and 800 rpm was applied to achieve better mass transfer and study the effect of rotation rate on the removal efficiency of Al. Effects of HF concentration on the removal efficiency of Al were conducted by using HF solutions of 1 %, 10 %, 20 %, and 40 % at 45 ℃, 800 rpm. In the ultrasound-aided removal experiments of Al, the effects of amplitude and frequency on removal efficiency of Al were studied with the calorimetric power of 45.78 W, 91.85 W, and 137.56 W at 45 ℃, and the frequency was fixed at 40 kHz, 80 kHz, and 120 kHz, respectively. Ice was regularly added to the water bath to control the temperature of the water bath. The leaching efficiency was evaluated by using the following equation:

$$\eta = C_t/C0 \times 100\% \quad (4)$$

where η is the removal efficiency of Al, %, Ct is the remaining content of Al in the Ti_3AlC_2 with the reaction time t, %, which was determined by testing the samples using the ICP-OES instrument. C_0 is the initial content of Al in the Ti_3AlC_2 powder, %.

After the removal of Al from Ti_3AlC_2 precursor, the slurry was repeatedly centrifugated at 3500 rpm for 3 min until the pH of the supernatant is close to 6.5 to remove adsorbed ions on the surface of the samples. Afterward, vacuum suction filtration of the resulting slurry is conducted to separate the acquired products from the aqueous solution.

Fabrication of the electrode is a necessary step for electrochemical performance tests, and the experimental details on the fabrication of the electrode can be found in our previous work[15]. The specific capacitance based on CV can be calculated by the following equation [16]:

$$C = \frac{\int IdU}{mv\Delta U} \quad (5)$$

where C (F/g) is specific capacitance in unit F/g; m is the mass of the active material used for preparing the electrode in unit g, v represents the CV scan rate, mV/s; ΔU (V) is the operating potential range of CV, V; I stands for the response current, A;

3. Results and discussion

3.1. Effect of operating parameters on removal efficiency of Al in absence and in presence of ultrasound

To evaluate the influence of ultrasound on the removal efficiency of Al, the effect of parameters on removal efficiency of Al in the absence and presence of ultrasound are studied (Fig. 1). In the experiments without ultrasound aid, it is vividly shown that the concentration of hydrofluoric acid plays an important role in removal efficiency, higher concentration favors the removal of Al, as shown in Fig. 1(a). In the 1 % HF solution, the removal efficiency of Al increases from 19.2 % for 4 h of etching to 41.5 % after 24 h of etching treatment. By comparison, the removal efficiencies of Al are over 90 % for 24 h of etching in the solutions with higher HF concentrations (10 %, 20 %, and 40 %). Of note, a sharp increase in the removal efficiency is observed as the timescale of reaction is less than 16 h, whereas the increasing rate of removal efficiency becomes slow with the etching time over 16 h. For example, a 14.4 % increase (from 74.7 % to 89.1 %) of removal efficiency is

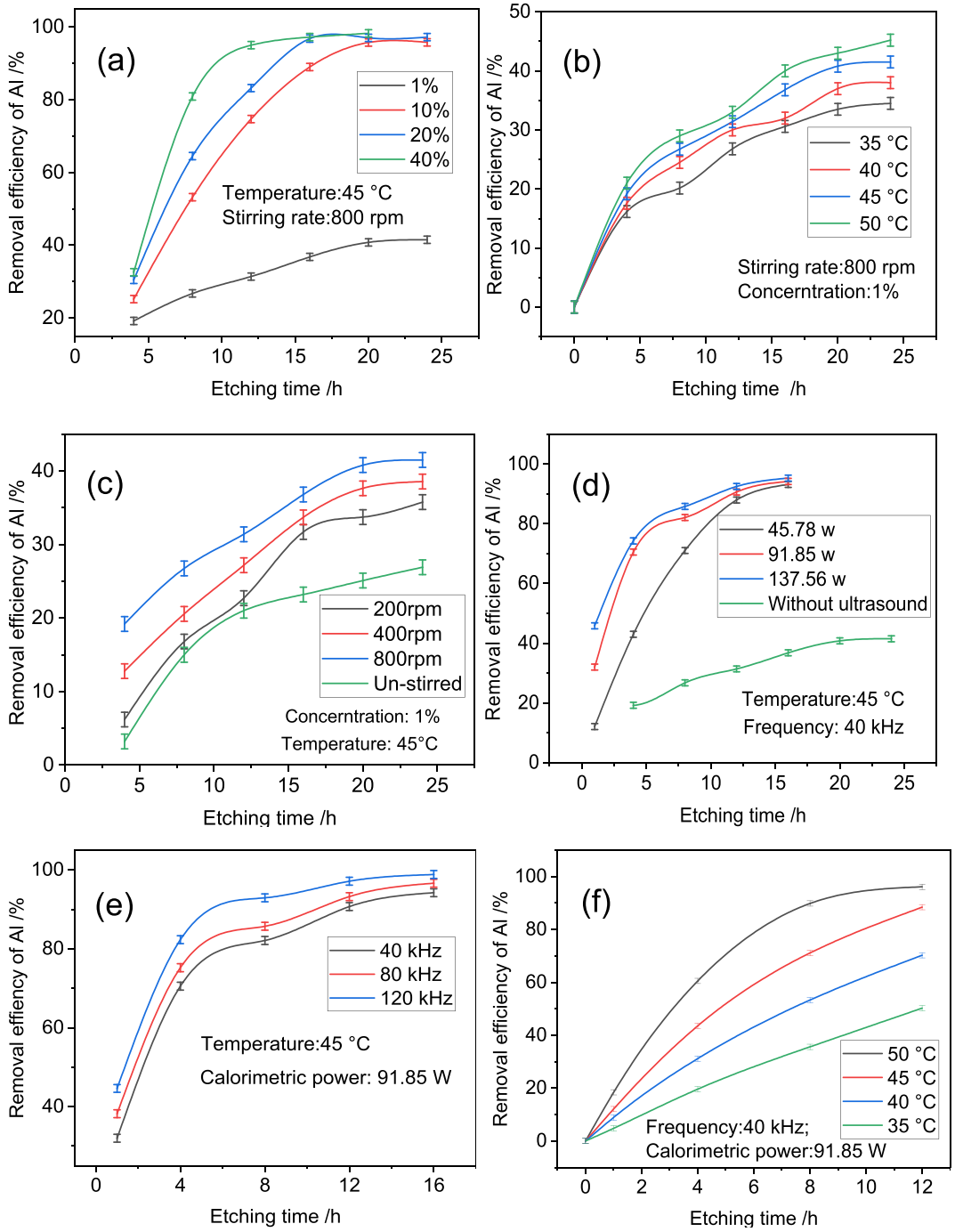

Fig. 1. Effects of operational parameters on removal efficiency of Al; (a):concentration effect; (b) temperature effect in absence of ultrasound; (c) effect of magnetic rotation rate; (d) effect of calorimetric power of ultrasound; (e) effect of applied frequency of ultrasound; (f) temperature effect in presence of ultrasound.

recognized as the removal time increases from 12 h to 16 h, relative to the 6.63 % (from 89.1 % to 95.73 %) of increase from 16 h to 20 h of removal of Al. The reason for this phenomenon is that the by-product (AlF_3) adheres to the surface of etched particles, according to the chemical reaction (1), which suppresses the further removal of Al. This is also in good agreement with our later discussion in the morphological study section of this work. The effects of temperature on the removal efficiency are shown in Fig. 1(b). As mentioned previously, we performed the removal experiments in the temperature range from 35 ℃ to 50 ℃ to avoid unwanted defects of the resulted MXenes. It is clearly shown that higher experimental temperature can promote the removal efficiency of Al. Taking 24 h of treatment as examples, the removal efficiencies of Al are 34.5 %, 38 %, 41.5 %, and 45.2 % at 35 ℃, 40 ℃, 45 ℃, and 50 ℃, respectively. Further discussion on the effects of temperature is available in the kinetic study section of this work. As stated above, the surface of the etched particles is covered by AlF_3, the by-product of the removal process of Al. Consequently, more intense agitation of the solution may be beneficial for the removal of the resulting by-product that covered the surface of the etched particulates. To confirm this information, the effect of stirring rate on removal efficiency of Al is studied, Fig. 1(c). As expected, higher Al removal efficiency is observed at 800 rpm, the highest rotation rate. Specifically, the removal rate of Al is 26.9 % in the unstirred solution for 24 h of removal of Al, while the corresponding values for 200 rpm and 800 rpm

experiments are 35.77 % and 41.5 %, respectively. It has to be stressed that a higher stirring rate not only can remove the surface-adhering by-products but also offers better mass transfer of the reactive species, which can promote the removal of Al from Ti_3AlC_2.

Regarding the experimental results in presence of ultrasound, three factors, the amplitude, and frequency of the applied ultrasound, as well as the temperature, are included. Among these, the amplitude of the applied ultrasound is represented by ultrasonic power in this work. Fig. 1(d) depicts the effect of ultrasonic power on the removal efficiency of Al. Herein, the corresponding calorimetric power densities are determined to be 45.78 W, 91.85 W, and 137.56 W for the applied ultrasonic power of 50 W, 100 W, and 150 W. It is impressively shown that the introduction of ultrasound can significantly boost the removal efficiency of Al. Specifically, the removal rates of Al for 16 h of reaction are all over 90 % with the applied ultrasonic calorimetric power of 45.78 W, 91.85 W, and 137.56 W. By comparison, the corresponding value for the experimental result in absence of ultrasound is 41.5 %. In addition, larger ultrasonic power corresponds to higher removal efficiency with the same etching time, e.g., in the case of 8 h of etching, the removal efficiencies of Al are 71.07 %, 82.10 %, 85.82 % with the applied ultrasonic calorimetric power of 45.78 W, 91.85 W, and 91.85 W, respectively. Higher ultrasonic power represents that more extra energy is provided by the sonicator, which can significantly improve the removal of Al. However, it is of note that excessive energy may cause undesirable defects of the resulted MXenes[12]. The effect of ultrasonic frequencies on the removal efficiency of Al is shown in Fig. 1(e), it is shown that the removal efficiency of Al is proportional to the applied frequency. A higher frequency can provide more opportunities for the etchant to attack the Ti_3AlC_2 precursor, which accelerates the removal of Al. The effect of temperature on the removal efficiency of Al is studied, and the results are shown in Fig. 1(f), it yields higher removal efficiency of Al at high experimental temperatures, which is analogous to the case without ultrasound. However, a close-to-linear increasing trend of the removal efficiency of Al with the etching time is observed, which is significantly different from those without ultrasound, and this indicates different kinetic mechanisms for the reaction process with and without ultrasound, i.e., the reaction pathways are different for the cases in absence of and presence of ultrasound: for the case in absence of ultrasound, AlF_3, the byproduct of the etching process, adhere to the surface of the MXenes, which hampered further etching of the samples. In contrast, the generated AlF_3 is removed by the ultrasound, thereby accelerating the removal of Al from Ti_3AlC_2 structures.

As stated above, in the temperature effect experiments, the removal efficiency of Al increases with the increase of the experimental temperature, significant difference is observed in Fig. 1(b) and (f), which necessitates further kinetic studies.

3.2. Kinetic considerations

Two classical models, namely shrinking core and shrinking particle models [17], have been proposed to further interpret the experimental data Fig. 1 (b) and (f). Of which the former describes a shrinking unreacted core but with solid resultants adhering to the etched particulates as proceeding of the removal of Al whilst the latter corresponds to the case of shrinking particles with no solid products adhering on the surface of the particulates. The two models can be mathematically expressed by the following equations [17]:

$$1 - (1 - x)^{1/3} = kt\,(Shrinking\ particle\ model) \tag{6}$$

$$1 - \frac{2}{3}x - (1 - x)^{2/3} = kt\,(Shrinking\ core\ model) \tag{7}$$

where x stands for the removal efficiency of Al, (%), k denotes the reaction rate constant, (h^{-1}), and t is the reaction time, (h).

The experimental data in Fig. 1 (b) and (f) were fitted by using both of the above equations. A better linear relationship is obtained with equation (7) in the case without ultrasound (Fig. 2(a)), whereas equation (6) is well suited to the experimental data in presence of ultrasound (Fig. 2(b)). That is, the removal of Al from Ti_3AlC_2 in absence of ultrasound obeys the shrinking core model, whilst the shrinking particle model is capable to describe the case in presence of ultrasound. In addition, the activation energies of the two cases are calculated by using the Arrhenius equation [18]:

$$k = Ae^{-E_a/RT} \tag{8}$$

where k represents the reaction rate constant, mol/(L·s); t stands for the reaction time, s; A is the frequency factor, mol/(L·s); E_a denotes the apparent activation energy, kJ/mol; R is the gas constant, 8.3145 J/K/mol; and T (K) is the absolute experimental temperature.

The Arrhenius plots of Fig. 2(a) and (b) are shown in Fig. 2(c) and (d), the activation energy of the reaction for the case without ultrasound aid is calculated to be 28.1 kJ/mol, which indicates a mixed kinetic feature of the reaction process, i.e., the removal efficiency of Al is controlled by both mass transfer and chemical reaction. According to our previous analysis and the definition of the shrinking core model, here the removal process specifically involves the following multiple steps:(i) the diffusion of reactant ions/molecules to the interface region of the HF solution and the solid Ti_3AlC_2 particles; (ii) adsorption of the reactant at the surface of Ti_3AlC_2 particles; (iii) the diffusion of resultants across the solid by-products, AlF_3; (iv) the diffusion of resultants from the by-product to the bulk solution. In contrast, the corresponding value for the reaction in presence of ultrasound is 70.2 kJ/mol, which demonstrates that the removal process of Al in presence of ultrasound is kinetically limited by chemical reaction, primarily because no by-products adhered on the surface of the etched particles.

3.3. Material characterization

Although the experimental results indicate distinct kinetic mechanisms for the cases with and without ultrasound. Further investigation is needed. Microscopic morphologies of the samples are observed by using FESEM, the corresponding figures in Fig. 3 (a) to (f) depict the SEM images for 4-, 8-, and 12-hour removal of Al in 10 % HF solution with the stirring rate of 800 rpm at 50 ℃. As predicted by the kinetic study in this work, ultrafine particles are readily observed on all three samples. According to our previous work[15], these ultrafine particles have been proved to be the byproduct of the reactions, AlF_3, which is insoluble in the as-employed solution. The microscopic morphologies of the etched with the same experimental conditions as those in Fig. 3(a) to (f) but in presence of ultrasound with the frequency of 40 kHz are shown in Fig. 3 (g) to (l). It is observed that no AlF_3 particles are present on the surface of the samples in presence of ultrasound. As analyzed in the kinetic study of this work, the shrinking particle model showed good capability in describing the case in in presence of ultrasound, i. e. no by-products of the reactions adhere on the surface of the samples. Consequently, the SEM observation in Fig. 3(g) to (l) is in good agreement with the kinetic study results.

Unlike other materials, the etched Ti_3AlC_2 exhibits accordioned-like morphology due to the selective removal of Al from the pristine Ti_3AlC_2 structure, which is consistent with the previous studies. It can be observed that the accordioned-like morphology is emerging for 4 h of etching treatment, and the thickness of the layers decreases with the increase of etching time, well-defined accordioned-like morphology of the samples is obtained with 12 h of etching.

Of note, more MXenes with a few-layered structure and smaller particle size were found in the ultrasonic-aided process, since the sonication process can provide extra energy for exfoliation of the MXenes with layered structures. As a consequence, MXenes with a smaller number of layers are exfoliated in the removal process of Al. To confirm this information, the 2 h etched sample treated with the ultrasound

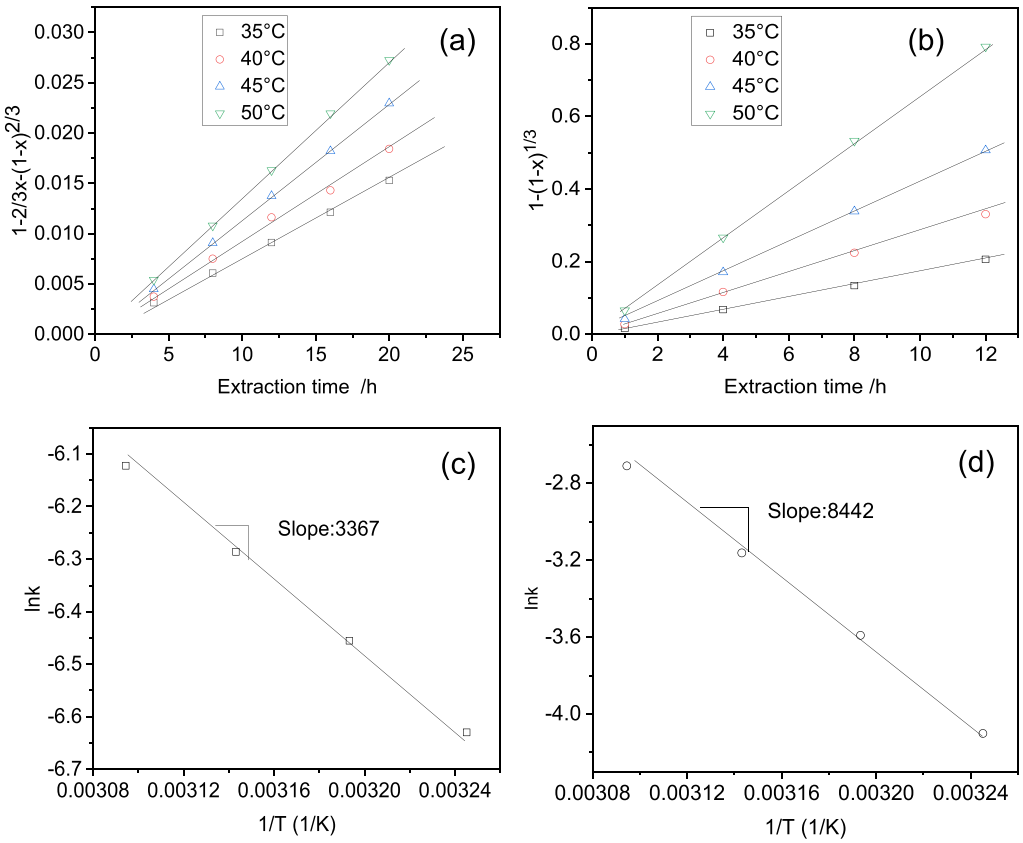

Fig. 2. (a) and (b): Plots of $1–2/3x-(1-x)^{2/3}$ and $1-(1-x)^{1/3}$ as a function of time for the removal of Al from Ti_3AlC_2; (c) and (d): the corresponding Arrhenius plots of Fig. 2(a) and (b).

calorimetric power and frequency of 137.56 W, 120 kHz is microscopically characterized. The corresponding micrographs are shown in Fig. 4 (a) to (d). MXenes with flower-like morphology are impressively observed in addition to the emerging accordioned-like morphology, which is a result of exfoliation of the multiple-layered MXenes.

In addition to SEM observation, the particle size of the pristine Ti_3AlC_2 and the samples with and without ultrasound treatment are measured. The results are shown in Fig. 5(a), (b), and (c), in which the average particle sizes are 21.3 μm, 18.5 μm, and 14.8 μm, i.e., the reduction of particle size is 2.8 μm after 2 h of treatment in absence of ultrasound whilst the corresponding value for the sample in presence of ultrasound is 6.5 μm, this agrees with the SEM observation and our previous analysis, i.e., the surface of the sample is covered by the resultant (AlF_3) and it gives larger particle size of the sample. By comparison, no solid products stand on the surface of the sample when ultrasound is introduced in the experimental process, offering a smaller particle size of the sample. Of note, the percentage of MXene with particle size less than ca. 5 μm is higher than those of the pristine and the sample without ultrasound treatment, this is attributed to the efficacy of ultrasound. The multiple-layered MXenes are exfoliated into flakes with smaller particle sizes, which are in good agreement with the SEM observation in Fig. 4.

As observed and what has been characterized in Figs. 4 and 5, the morphology and particle size distribution of the sample with and without sonication are different due to the intervention of ultrasound. Specific area determination of the samples is of particular interest (Fig. 6). The specific area for Ti_3AlC_2 is calculated to be 2.1 m^2/g, and the small increase of the black line in Fig. 6 corresponds with the solid structure that is not accessible to the N_2 gas. The specific area for Ti_3C_2Tx with and without ultrasound treatment is calculated to be 13.6 m^2/g and 21.7 m^2/g, respectively. The larger specific area of the etched samples is ascribed to the removal of Al from the Ti_3AlC_2 structures, thereby producing organ-like morphology of the samples. Hysteresis loops are observed in Fig. 6 in the relative pressure range from 0.5 to 1.0, which is produced by the mesopores and macropores in the samples. In addition, compared with the sample without ultrasound treatment, the hysteresis loops are more prevalent for the sample in presence of ultrasound than that of the sample in absence of ultrasound. The larger specific area of the sample with sonication treatment demonstrates a more effective removal of Al than that for the sample in absence of ultrasound.

In addition to particle size distribution and the specific area, special attention to the effect of ultrasound on the phase composition of the MXene should be paid. The XRD patterns of the samples with and without sonication treatment are shown in Fig. 7(a) and (b). It is shown in Fig. 7(a) that the (002) and (104) peaks of the pristine Ti_3AlC_2 at 9.8°, and 39.4° [19], lose intensity with the increase of the reaction time, which demonstrates that Al was removed from the Ti_3AlC_2 precursor. Of note, the above-mentioned (002) peak shifts to the lower angle with the increase of reaction time, this is ascribed to the broadened interlayer of the samples due to the removal of Al atoms. Regarding the XRD patterns in presence of ultrasound treatment, besides the above-mentioned losing intensity and left-shifting feature, the peaks for the samples shown in Fig. 7(b) are more broaden than those of the samples without ultrasound treatment, which indicates a smaller grain size of the resulting MXenes of the ultrasonically treated samples than those for the samples without ultrasound treatment, and the MXenes with smaller grain size are generated under the impact of ultrasound in the reaction process, i.e., the generated MXene particulates can be damaged by the applied ultrasound.

3.4. Effect of ultrasound on energy storage mechanism of Ti_3C_2Tx MXene

As stated in the introduction section, energy storage accounts for one

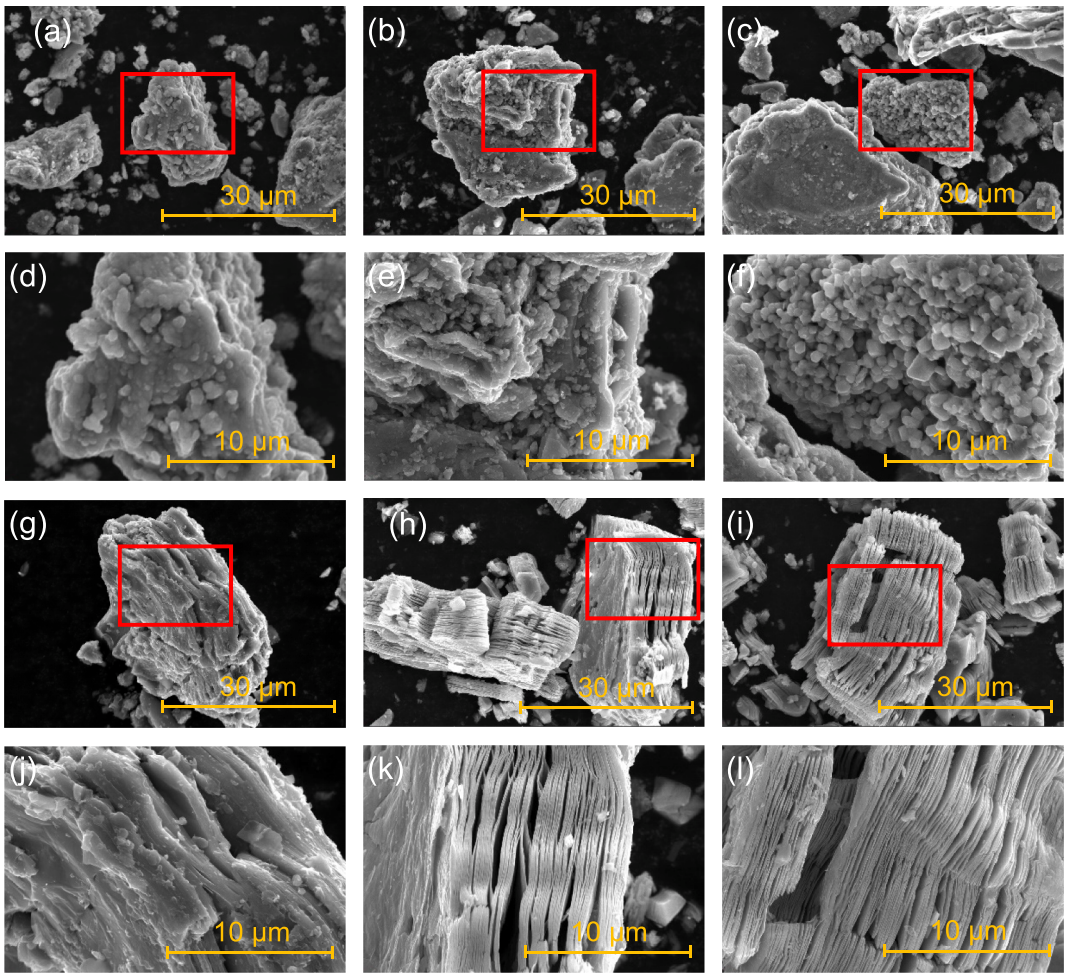

Fig. 3. Effect of etching time on micrographic morphology of the samples Al etched by using 10 % HF solution at 800 rpm, 45 ℃. (a) and (d): 4 h, (b) and (e); 8 h (c) and (f) 12 h; and the corresponding morpholgy of the samples with ultrasound aid at 40 kHz, 91.85 W, 45 ℃ (g) and(j) 4 h, (h) and (k) 8 h; (i) and (l) 12 h.

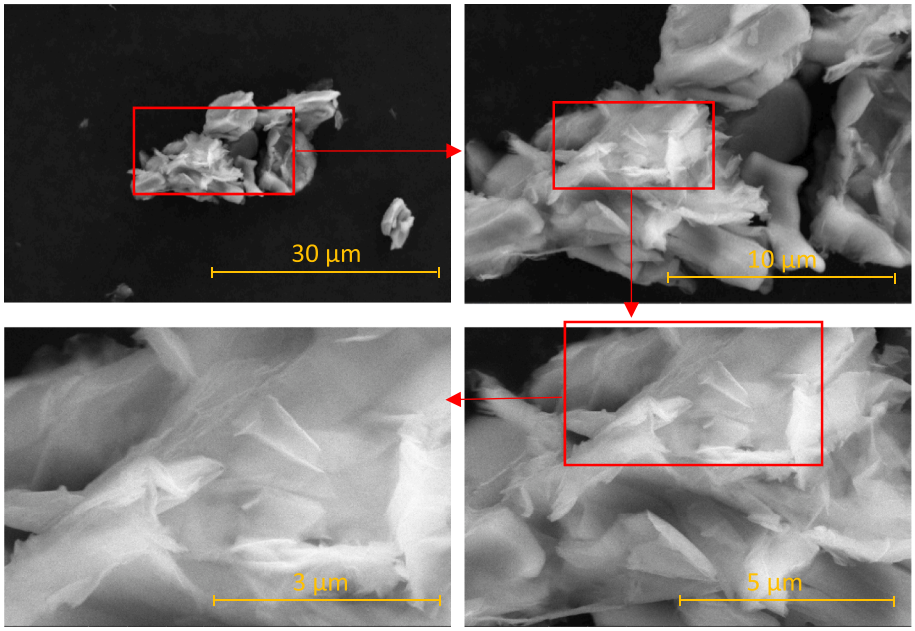

Fig. 4. Micrographs of the sample treated with the ultrasonic calorimetric power and frequency of 137.56 W, 120 kHz at 50 ℃.

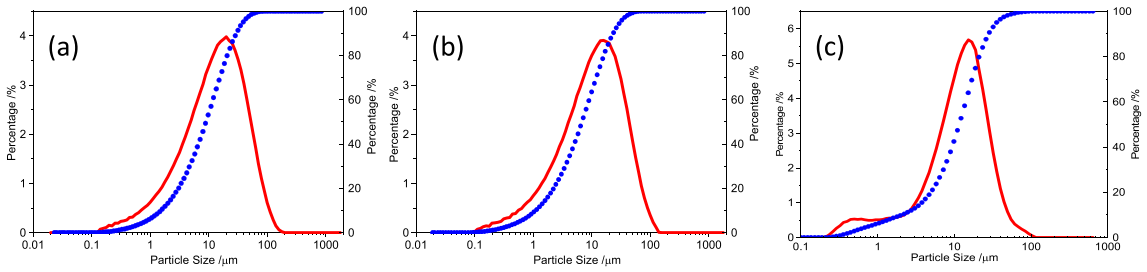

Fig. 5. Particle size distribution of the samples (a: the pristine Ti_3AlC_2; b: treated by using 10 % HF solution for 6 h, 45 ℃ without ultrasonic aid and c: with ultrasonic aid at 137.56 W, 120 kHz).

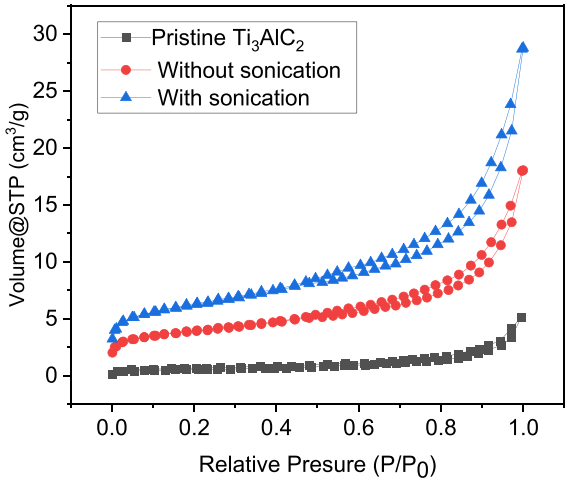

Fig. 6. N_2 adsorption/desorption isotherm curves of the samples (black line: the pristine Ti_3AlC_2; blue line: treated by using 10 % HF solution for 6 h, 45 ℃ without ultrasonic aid and red line: with ultrasonic aid at 137.56 W, 120 kHz).

of the major applications of MXenes. The effect of ultrasound on the energy storage mechanism of Ti_3C_2Tx MXene is of particular interest. The cyclic voltammograms(CV) with different scan rates by using the samples with and without sonication is shown in Fig. 8(a), (b) and (c). The sample with ultrasound treatment possesses much larger specific capacitance than the ones without ultrasonic aid, which is in good agreement with our previous study [15]. In addition, the sonication calorimetric power of the samples corresponding to Fig. 8(a), (b), and (c) are 0 W, 91.85 W, and 137.56 W. The specific capacitance of the samples increases with the increase of ultrasonic power. For example, the specific capacitances of the samples in Fig. 8(a) and (b) are calculated to be 28.39 F/g 98.29 F/g, and 128.21 F/g at 10 mV/s, respectively. Interestingly, the CVs of the sample with ultrasound treatment exhibit a close-to-rectangular shape, without current peaks observed, which is a typical characteristic for double-layer capacitor materials. With the intervention of ultrasound, the CV deviates from the rectangular shape significantly with the increase of ultrasonic power. The CVs of the samples with ultrasound treatment exhibit current peaks which are produced by the redox reaction of Ti atoms in the Ti_3C_2Tx structure. This indicates that ultrasound can influence the energy storage mechanism of the Ti_3C_2Tx. Mechanically, the total capacitance of MXenes can be divided into two components: (i) surface confined capacitance and (ii) diffusion limited capacitance. The former includes double layer capacitance and pseudocapacitance produced by surface redox reaction, while the latter denotes the pseudocapacitance which is limited by ion diffusion. Dunn et al. proposed a method to quantitatively evaluate the contribution of the above-mentioned surface-confined and diffusion-limited capacitance, which can be represented by the following equation[20]:

$$i(V) = k_1 v + k_2 v^{1/2} \quad (9)$$

where $i(V)$ is the current at characteristic potential; (A), v is the scan rate (mV/s) of CV, $k_1 v$ and $k_2 v^{1/2}$ represent the capacitive and diffusion-limited processes, respectively. k_1 and k_2 are two adjustable constants.

Further interpretation of the CVs shown in Fig. 8(a), (b), and (c) based on equation (9) is shown in Fig. 8(d). The different energy storage mechanism of the samples is readily observed: the sample without sonication treatment possess 100 % surface confined capacitance, whilst the samples prepared in presence of sonication exhibit both surfaces confined capacitance and diffusion-limited capacitance. Specifically, the contribution of surface-confined capacitance increases with the scan rate of CVs for the ultrasound-treated samples. In addition, with the increase of ultrasonic power, a decrease in diffusion-limited capacitance is observed with the same scan rate of CV. For example, the diffusion-limited accounts for 10 % of the total capacitance for the 91.85 W ultrasonic treatment sample at 100 mV/s, while it decreases to 1 % as the ultrasound calorimetric power increases to 137.56 W.

In addition to the above description, surface terminations affect the

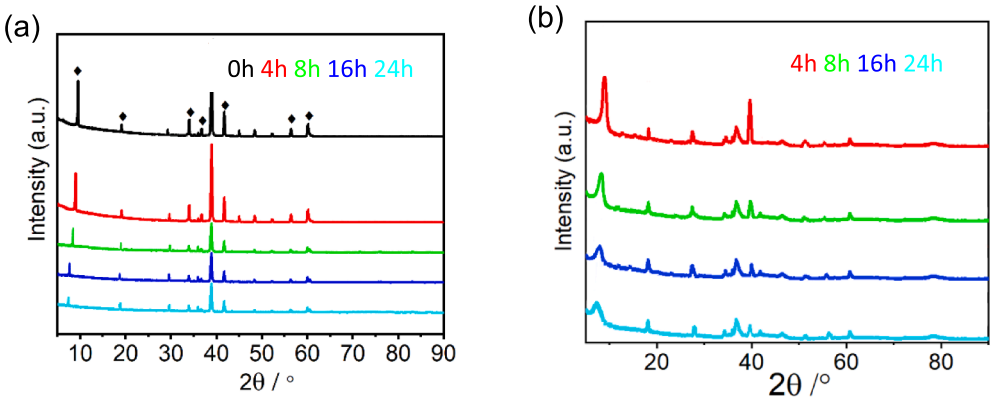

Fig. 7. Effect of reaction time on XRD patterns of the samples (a: 45 ℃, 800 rpm; b: 45 ℃, 120 kHz, calorimetric power:137.56 W).

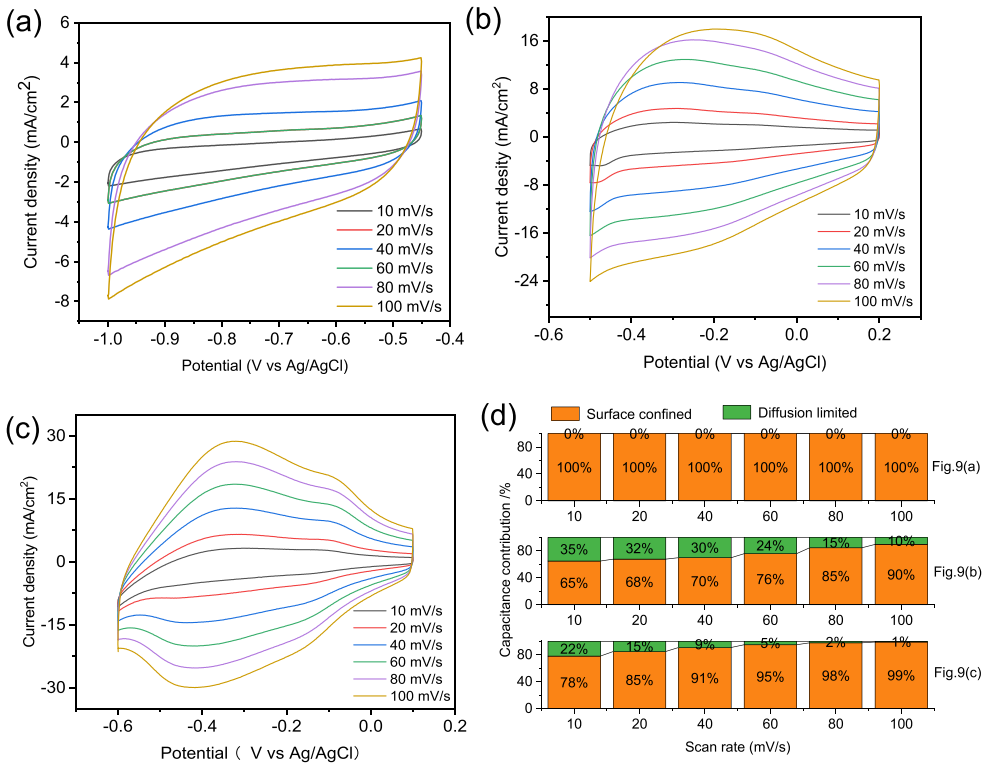

Fig. 8. (a), (b) and (c): Cyclicvoltammograms of the samples in 1 M H_2SO_4 by using the samples treated in 10 % HF for 12 h at 45 ℃ (experimental condition: (a): magnetically stirred at 800 rpm; (b): sonication at 120 kHz, 91.85 W; (c): sonication at 120 kHz, 137.56 W); (d): plots of the contribution of capacitive and diffusion behaviors of the samples shown in Fig. 8(a), (b), and (c).

energy storage mechanism of the resulting Ti_3C_2Tx MXene. Rich surface chemistry is unique merit of MXene materials. The effect of ultrasound on the variation of surface chemistry of the samples is an important issue to be considered in addition to the removal efficiency of Al for synthesizing Ti_3C_2Tx MXene. Herein, XPS characterization is performed for the 4 h etched samples at 45 ℃ with and without ultrasound aid in the etching process. The XPS survey of the two samples is shown in Fig. 9(a). As intuitively predicted from the chemical composition of Ti_3AlC_2 precursor, Al 2p, C 1s, and Ti 2p peaks were detected at 74.93 eV, and 284.8 eV, respectively[21]. Other peaks at 529.10 eV and 684.01 eV observed in Fig. 9(a), which correspond to the O1s and F1s, are recognized [22]. Compared with the sample without ultrasound aid in the etching process, no new peaks are observed in the sample with sonication treatment. High-resolution spectra are also performed to further study the surface chemistry of the samples. C—C, C—Ti, C—O, and C═O chemical bonds at 280.98 eV, 284.6 eV, 286.08 eV, and 288.46 eV are detected in the high-resolution C 1s spectrum 4 h etched sample without ultrasound [23]. By comparison, C-Ti chemical bond is absent from the high-resolution C1s spectrum of the 4 h etched sample in presence of ultrasound, indicating the deforming of C-Ti bond with the intervention of ultrasound. C═O bond with the binding energy of 287.52 eV emerged as a new bond in the sample with sonication, manifesting more rigorous oxidation of C in the sonication-assisted process of etching. This is a result of the deformation of C-Ti bond, after which both the exposed Ti and C atoms are oxidized. It has been reported that oxygen-containing groups such as ═O, —O—C═O, and –OH, can promote the electrochemical performance of MXenes via surface redox reactions [24]. Regarding the Ti 2p spectrum, Ti-Al and C-Ti chemical bonds, with the binding energy of 453.6 eV and 454.47 eV [25], are detected, while no peaks associated with Ti-Al and C-Ti chemical bonds are observed in the sonication-assisted etched sample. This phenomenon demonstrates higher removal efficiency in the sonication-assisted approach, which is consistent with the experimental results shown in Fig. 1. It was reported that the Ti atoms in Ti_3AlC_2 structure are closer to +2 rather than +4, Ti-O 2p1/2 and 2p3/2, corresponding to the binding energy of 460.06 eV and 456.04 eV[13], are therefore detected in the sample without sonication-aid but not found in the ultrasound-aided etched sample. The above-mentioned TiO 2p3/2 peak disappeared. Instead, the Ti_2O_3 2p1/2 and 2p3/2 in the ultrasound-aided etched sample are observed with the binding energy of 460.02 eV and 457.58 eV [26], this manifests more rigorous oxidation of Ti atoms in the case of ultrasound-aided approach. Noteworthy, Ti_3C_2Tx exhibits the typical nature of 2D materials, the oxidation starts from the outermost surface layer and the outer edges of the Ti_3C_2Tx, which gives rise to the more broadened and convoluted Ti 2P spectra of the Ti_3C_2Tx sample than those of the normal Ti-based materials. In addition, the peaks of TiO_2 (2p3/2 and 2p1/2, 458.55 eV and 463.11 eV, [27]) and Ti-F (464.42 eV, [15]) chemical bonds are also detected in both of the two samples, indicating surface terminating of the samples by –OH and -F groups. High-resolution F 1s spectra of the two samples are shown in Fig. 9(f) and (g). In Fig. 9(f), F-Ti and F-Al chemical bonds with the binding energy of 285.2 eV and 686.9 eV are observed[24], of which the former is attributed to the surface termination of -F group and the latter corresponds to the AlF_3 by-products of the reaction (1) in this work, which is observed in the section of SEM observation section in this work, the XPS experimental results are in good agreement with the SEM observation. Regarding the F1s spectra of the sample in presence of ultrasound, F-Ti chemical bond is the only chemical bond, which indicates surface termination of the sample by -F group.

4. Conclusion

In this study, the effect of ultrasound on the removal of aluminum from Ti_3AlC_2 and the electrochemical performance of the resulting Ti_3C_2Tx MXene was evaluated. In the Al removal process, it was experimentally verified that both higher ultrasonic power and frequency can promote the removal efficiency of Al, of which the ultrasonic power exhibited more impact than the frequency of the applied ultrasound.

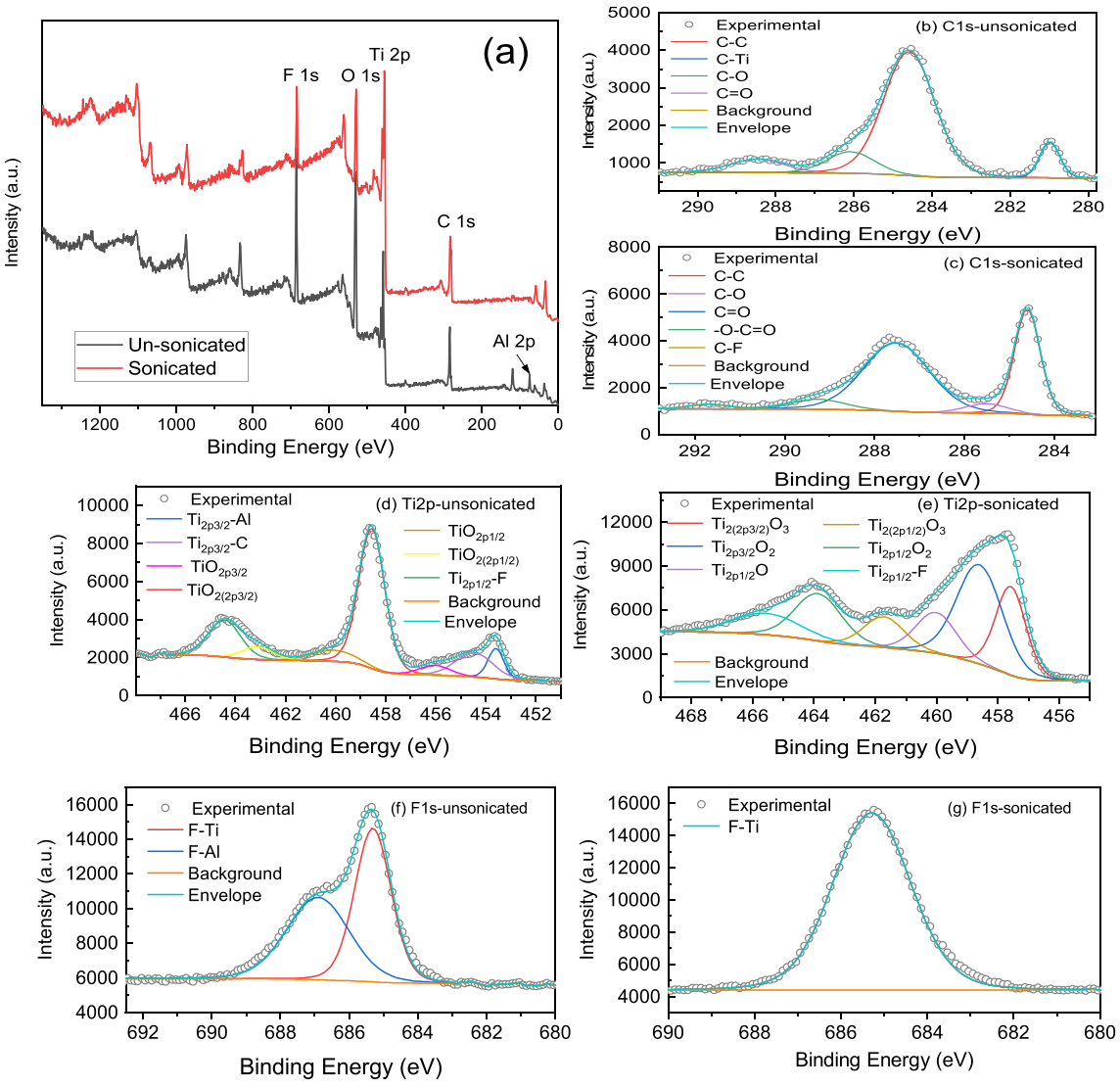

Fig. 9. XPS characterization results of the samples with and without sonication aid (etching time: 12 h, experimental temperature: 45 ℃, ultrasonic frequency and calorimetric powder: 80 Hz, 91.85 W).

Application of ultrasound can remove the surface adhering AlF_3, the by-product for Al removal process, which led to significant distinct kinetics removal process of Al: the reaction process with ultrasonic aid obeyed the shrinking particle model, whilst the shrinking particle model was used to describe the removal of Al in presence of ultrasound. In addition, the reaction process with the aid of ultrasound, with the activation energy of 70.2 kJ/mol, was identified to be kinetically controlled by chemical reaction. The reaction process with and without ultrasound was calculated to be 28.1 kJ/mol, with the mixed kinetic feature in the reaction process. Ultrasound favors the generation of few-layered MXene with flower-like morphology, which exhibited larger specific area, smaller particle size, and smaller grain size than their multiple-layered counterparts. The samples with ultrasound aid in the fabrication process have better electrochemical performance than those ones without sonication assistance. It was verified that introduction of ultrasound can significantly increase the specific capacitance of the samples. Specifically, the specific capacitance of the sample without ultrasound exhibits pure specific capacitance of 28.39 F/g at 10 mV/s, whilst it possesses both surfaces confined and diffusion-limited capacitances with a value of 128.21F/g for the sample fabricated in presence of sonication.

CRediT authorship contribution statement

Wu Zhang: Supervision, Funding acquisition, Writing – review & editing, Validation, Project administration, Writing – original draft. **Xinyue Zhang:** Conceptualization, Methodology, Data curation, Visualization, Investigation.

Declaration of Competing Interest

The authors declare that they have no known competing financial interests or personal relationships that could have appeared to influence the work reported in this paper.

Data availability

Data will be made available on request.

Acknowledgements

The authors gratefully acknowledge the financial support from the Department of Science and Technology of Liaoning Province, China (2019-ZD-0261) and the financial support from the Department of

Education of Liaoning province, China (LJKZ0250).

References

[1] X. Xu, Y. Zhang, H. Sun, J. Zhou, F. Yang, H. Li, H. Chen, Y. Chen, Z. Liu, Z. Qiu, D. Wang, L. Ma, J. Wang, Q. Zeng, Z. Peng, Progress and perspective: MXene and MXene-based nanomaterials for high-performance energy storage devices, Adv. Electron. Mater. 7 (2021) 2000967.

[2] A. VahidMohammadi, J. Rosen, Y. Gogotsi, The world of two-dimensional carbides and nitrides (MXenes), Science 372 (2021) 1165.

[3] Y. Tang, C. Yang, X. Xu, Y. Kang, J. Henzie, W. Que, Y. Yamauchi, MXene nanoarchitectonics defect-engineered 2D MXenes towards enhanced electrochemical water splitting, Adv. Energy Mater. 12 (2022) 2103867.

[4] W.L. Ding, Y.H. Cao, H. Liu, A.X. Wang, C.J. Zhang, X.R. Zheng, In situ growth of NiSe@$Co_{0.85}$Se heterointerface structure with electronic modulation on nickel foam for overall water splitting, Rare Metals 40 (2020) 1373–1382.

[5] Z. Feng, T. Shi, W. Liu, W. Zhang, H. Zhang, Highly active bifunctional electrocatalyst: Nanoporous (Ni, Co)0.85Se anchored on rGO for water and hydrazine oxidation, Int. J. Energy Res. (2022), https://doi.org/10.1002/er.8292.

[6] Z. Feng, E. Wang, S. Huang, J. Liu, Bifunctional nanoporous Ni-Co-Se electrocatalyst with superaerophobic surface for the water and hydrazine oxidation, Nanoscale 12 (2020) 4426.

[7] Y.Z. Wang, Y.M. Ding, C.H. Zhang, B.W. Xue, N.W. Li, L. Yu, Formation of hierarchical Co-decorated Mo_2C hollow spheres for enhanced hydrogen evolution, Rare Metals 40 (2021) 2785–2792.

[8] N. Sheikh, M.B. Tahir, N. Fatima, M. Sagir, M. Pervaiz, M.S. Tahir, Recent advances in the rational design of 2D MXenes in energy conversion and storage systems, Int. J. Energy Res. 45 (2021) 17563–17576.

[9] J. Chen, Y. Ding, D. Yan, J. Huang, S. Peng, Synthesis of MXene and its application for zinc-ion storage, SusMat 2 (2022) 293–318.

[10] O. Mashtalir, M. Naguib, B. Dyatkin, Y. Gogotsi, M.W. Barsoum, Kinetics of aluminum extraction from Ti_3AlC_2 in hydrofluoric acid, Mater. Chem. Phys. 139 (2013) 147–152.

[11] X. Li, M. Li, Q. Yang, G. Liang, Z. Huang, L. Ma, D. Wang, F. Mo, B. Dong, Q. Huang, C. Zhi, In situ electrochemical synthesis of MXenes without acid/alkali usage in/for an aqueous zinc ion battery, Adv. Energy Mater. 10 (2020) 2001791.

[12] M. Malaki, A. Maleki, R.S. Varma, MXenes and ultrasonication, J. Mater. Chem. A 7 (2019) 10843–10857.

[13] M. Shen, W. Jiang, K. Liang, S. Zhao, R. Tang, L. Zhang, J.Q. Wang, One-pot green process to synthesize MXene with controllable surface terminations using molten salts, Angew. Chem. Int. Ed. 60 (2021) 27013–27018.

[14] M. Alhabeb, K. Maleski, B. Anasori, P. Lelyukh, L. Clark, S. Sin, Y. Gogotsi, Guidelines for synthesis and processing of two-dimensional titanium carbide ($Ti_3C_2T_x$ MXene), Chem. Mater. 29 (2017) 7633–7644.

[15] X. Zhang, W. Zhang, H. Zhao, Ultrasound-assisted fabrication of $Ti_3C_2T_x$ MXene toward enhanced energy storage performance, Ultrason. Sonochem. 86 (2022), 106024.

[16] W. Wu, D. Wei, J. Zhu, D. Niu, F. Wang, L. Wang, L. Yang, P. Yang, C. Wang, Enhanced electrochemical performances of organ-like Ti_3C_2 MXenes/polypyrrole composites as supercapacitors electrode materials, Ceram. Int. 45 (2019) 7328–7337.

[17] Bowen Zhu,, Yingjie Zhang, Yuling Zou, Zelong Yang, Bao Zhang, Yan Zhao, Mingyu Zhang, Qi Meng, Peng Dong, Leaching kinetics and interface reaction of $LiNi_{0.6}Co_{0.2}Mn_{0.2}O_2$ materials from spent LIBs using GKB as reductant. J. Environ. Manage. 300 (2021) 113710.

[18] H. Wang, Z. Li, Q. Meng, J. Duan, M. Xu, Y. Lin, Y. Zhang, Ammonia leaching of valuable metals from spent lithium ion batteries in NH_3-$(NH_4)_2SO_4$-Na_2SO_3 system, Hydrometallurgy 208 (2022), 105809.

[19] J. Li, X. Yuan, C. Lin, Y. Yang, L. Xu, X. Du, J. Xie, J. Lin, J. Sun, Achieving high pseudocapacitance of 2D titanium carbide (MXene) by cation intercalation and surface modification, Adv. Energy Mater. 7 (2017) 1602725.

[20] J. Wang, J. Polleux, J. Lim, B. Dunn, Pseudocapacitive contributions to electrochemical energy storage in TiO_2 (anatase) nanoparticles, J. Phys. Chem. C. 111 (2007) 14925–14931.

[21] W. Bao, L. Liu, C. Wang, S. Choi, D. Wang, G. Wang, Facile synthesis of crumpled nitrogen-doped MXene nanosheets as a new sulfur host for lithium-sulfur batteries, Adv. Energy Mater. 8 (2018) 1702485.

[22] C. Feng, Z. Zhao, C. Luo, Y. Wang, X. Wu, W. Chen, Electrochemical storage mechanism of interstratification-assembled $Ti_3C_2T_x$ MXene/NiCo-LDHs electrode in alkaline, acid and neutral electrolytes, Ceram. Int. 48 (2022) 3884–3894.

[23] V. Kamysbayev, A.S. Filatov, H. Hu, X. Rui, F. Lagunas, D. Wang, R.F. Klie, D. V. Talapin, Covalent surface modifications and superconductivity of two-dimensional metal carbide MXenes, Science 369 (2020) 979–983.

[24] Y. Dall'Agnese, M.R. Lukatskaya, K.M. Cook, P.-L. Taberna, Y. Gogotsi, P. Simon, High capacitance of surface-modified 2D titanium carbide in acidic electrolyte, Electrochem. Commun. 48 (2014) 118–122.

[25] K. Li, T. Xiong, J. Liao, Y. Lei, Y. Zhang, W. Zhu, Design of MXene/graphene oxide nanocomposites with micro-wrinkle structure for efficient separating of uranium (VI) from wastewater, Chem. Eng. J. 433 (2022), 134449.

[26] S. Yang, P. Zhang, F. Wang, A.G. Ricciardulli, M.R. Lohe, P.W.M. Blom, X. Feng, Fluoride-free synthesis of two-dimensional titanium carbide (MXene) using a binary aqueous system, Angew. Chem. Int. Ed. 60 (2021) 8689–8693.

[27] F. Liu, A. Zhou, J. Chen, J. Jia, W. Zhou, L. Wang, Q. Hu, Preparation of Ti_3C_2 and Ti_2C MXenes by fluoride salts etching and methane adsorptive properties, Appl. Surf. Sci. 416 (2017) 781–789.